06

Studying the dynamics of drying droplets using a graphene sensor

© V.A. Andryushchenko,[1] I.A. Betke,[2] A.I. Bogomolova,[1] D.V. Sorokin[1]

[1]Kutateladze Institute of Thermophysics, Siberian Branch, Russian Academy of Sciences,
630090 Novosibirsk, Russia
[2]Novosibirsk State University,
630090 Novosibirsk, Russia
e-mail: vladimir.andryushchenko@gmail.com

Received October 1, 2024
Revised October 1, 2024
Accepted October 1, 2024

The evaporation of water droplets on graphene sensors, which are a non-conductive substrate made of silicon dioxide with graphene deposited on it, obtained by chemical vapor deposition, as well as copper electrodes deposited by magnetron method, is studied. It is shown that a water droplet deposited on the sensor surface changes its conductivity as it evaporates. The dependences of the resistance of the graphene sensor on the geometric characteristics of the droplet (height, contact angle, contact area of the droplet with the surface) are established. The sensitivity of the sensor to determining the evaporation mode of the droplet is demonstrated.

Keywords: graphene, conductivity, water droplet, sensor.

DOI: 10.61011/TP.2025.02.60818.301-24

Introduction

Development of IoT and smart home concepts as well as transition to precision medicine and high-tech healthcare necessitated the development of various smart sensor technologies. Considerable success has been currently achieved in the field of optical and sound sensors [1]. It can be quite safely said that an „electronic eye“ and „electronic ear“ have been created successfully [1]. So far, a similar success in creating an „electronic tongue“ and „electronic nose“ hasn't been achieved yet [2]. The main problem here is the need to maintain high recognition accuracy and rate for small impurities that define effective use of these systems for real applications such as express diagnosis of infectious human diseases, atmosphere composition monitoring, food quality monitoring, etc. [3]. Moreover, sensors shall be created in maximum compact design. The existing studies in this area demonstrated the need for developing new functional materials for high-performance sensors [4]. Utilization of carbon materials, in particular, graphene and its derivatives, has been actively considered in the past decade as one of potential solutions [5,6].

Graphene is an ideal candidate for the role of a carrying surface for various sensors because it has high strength properties, chemical and thermal resistance, and high thermal and electrical conductivity coefficients. At the same time, graphene is a promising material for a wide range of various applications associated with modification of chemical and physical surface properties [7,8]. Graphene coatings may be used effectively for surface protection against aggressive environmental effect and can also change the lyophilic behavior of a surface [9]. There are quite many potential applications of graphene and its derivatives.

Sensor properties of graphene materials cause a special interest due to their unique two-dimensional structure, large specific surface area and high conductivity [10–17]. Two-dimensionality of graphene automatically provides a compact size of a future graphene sensor. Physical elasticity of graphene may be helpful in creating flexible sensors. Graphene may be also functionalized in various ways to help achieve high selectivity of created devices and their sensitivity to a wide range of various analytes. Carbon atoms that form graphene are able to absorb gas molecules providing a large analysis zone and high sensitivity [17]. Interaction between graphene and adsorbates may vary from weak Van der Waals interactions to strong covalent bonding. These interactions may change graphene's electronic system significantly. Thus, graphene's two-dimensionality ensures electronic structure sensitivity even to the occurrence of single analyte molecules [18].

As mentioned above, the interest in studying graphene is associated with its unique physical properties. However, a zero band gap is the main obstacle in the path of graphene application in semiconductor electronics. Several potential methods to create a band gap in graphene and control its width are currently distinguished. They may include formation of graphene nanoribbons (narrow graphene ribbons about 10 nm in width) and graphene functionalization [19–21]. The first method allows the band gap width to be controlled by varying the graphene cutting pattern [20]. The second method — graphene functionalization — implies graphene surface binding with other types of atoms [22,23]. For example, when hydrogen, fluorine or boron atoms are bound to the graphene's carbon atoms, graphane, fluorographane and borophene are produced, respectively. The band gap opening width in this case is defined by the surface functionalization level [24].

Due to varying the band gap width during functionalization, one of the possible future graphene applications includes its utilization as a gas sensor — a sensing element that can measure the composition of a gas mixture [25] and atmospheric moisture [26]. Modification of graphene properties in such sensors is carried out by chemical adsorption of atoms. Operating principle of such sensors is based on the fact that when such sensor is placed in a gas medium, gas molecule adsorption occurs on the sensor surface thus changing the graphene sensor resistance [26]. To remove gas particles from the graphene surface, higher current is applied through the graphene to heat the surface and desorb gas molecules [18]. Thus, graphene-based sensors may be reusable [27]. However, sensor sensitivity is affected by a whole range of factors such as sensor substrate material [28], number of graphene layers [29], defects [30], etc. Main behaviors observed in such sensors are caused by the interaction of single molecules of various substances with graphene and their effect on graphene's electrical properties. This question is discussed actively by various teams [31–36]. The role of environment, number of layers and defects in graphene, presence and material of the substrate [28,37], temperature [38], etc., is discussed most actively. Despite the active discussion, no consistent theory describing the influence of single molecules on the electrical properties of graphene have been constructed so far, and all existing data was obtained either experimentally or by means of molecular-dynamic modeling according to density functional theory [28,32–34,38].

To create such systems, CVD-graphene is often used because the CVD-synthesis techniques produce single-layer graphene films with various designs and graphene layer structure [39]. One of the key advantages of these techniques is their scalability and possibility to create functional coatings with controlled properties on the basis of CVD-graphene. However, there is experimental and theoretical data, from which it follows that graphene properties are extremely sensitive to the ambient moisture [40]. This fact has a positive effect in terms of development of sensing equipment for moisture measurement and a negative effect in terms of instability of the physical properties of functional graphene coatings when atmosphere composition is varied.

Interaction between graphene with water molecules and various gases was studied experimentally in [18,27], however, the results are controversial. Study [18] investigated the effect of adsorption of the NO_2, H_2O, iodine (acceptors) and NH_3, CO, ethanol (donors) molecules with a concentration of $1\,cm^3/m^3$ on the surface conductivity of a mechanically split graphene monolayer on oxidized silicon, and showed that the conductivity is proportional to the concentration of charge carriers ($\Delta\sigma \propto \Delta n$), and the carrier mobility ($\mu \approx 5000\,cm^2/(V{\cdot}s)$) remains unchanged. This work shows that the sample resistance during interaction with water vapor decreases by approx. 1%. Opening of the graphene band gap as a result of water adsorption on the surface is reported in [27]. It is also shown in [27] that, during interaction with water vapor, the sample resistance grows by 38, 65%, 114% and 154% with respect to the sample resistance in vacuum for moisture levels 0.022 kg/kg, 0.065 kg/kg, 0.152 kg/kg and 0.312 kg/kg, respectively.

Models that would describe typical state of a graphene surface coated with a solid liquid layer are currently not reported in the literature. Possible applications of water-charged graphene may also include heat transfer enhancement in various MEMC (Motion Estimation and Motion Compensation) devices [41], water treatment [42], including without creating membranes [43], microscale and macroscale wettability control [44], etc.

Modern concepts of wettability of graphene coatings also have some contradictions associated with the aspects of wettable graphene transparency [45] and the graphene coating effect on contact angle variation [46]. Wettability affects significantly not only the contact angle, but also surface distribution, water drop size and morphology on the graphene surface [47]. Note also that for surfaces coated with a solid liquid layer, not only interactions between water molecules and graphene, but also interactions between water molecules start playing a significant role. This interaction provides additional liquid structuring in surface layers. Water structuring near graphene surfaces has been actively studied in recent years both using a molecular dynamics method [48–50] and experimentally [51]. Possible control of liquid structure in a surface layer by varying an electric field normal to the surface is also discussed in [49]. However, correlation of water molecule structuring with graphene's electronic structure is not discussed in these works. Thus, surface wettability depends not only on direct interaction between graphene atoms and water molecules, but also on the presence and configuration of external electric fields induced in the surface zone. Understanding the effect of these fields on liquid molecule layout may offer a possibility to control graphene coating wettability using normal and tangential electric fields.

Several years ago, it was found that, when a graphene sensor was successively immersed in water and then dried, its conductivity changed in the same successive manner [52]. Moreover, it turned out that graphene is sensitive not only to the presence of liquid, but also to the presence of liquid flow [53]. This effect may be used to make liquid motion sensors that don't affect the properties of initial flows too much, etc. Moreover, electric power generation by means of liquid motion along the graphene surface may be a promising application of interaction between graphene and liquid flow [54]. Various potential mechanisms of electric current excitation in a graphene plane are currently discussed. One of the reasons why electric current is excited in a graphene plane may be the interaction between graphene and charges and dipoles in the liquid flow induced at the graphene surface [55]. However, mechanisms that define effective conversion of liquid motion energy into electric power have not been studied so far and are still the matter of extensive discussions. Possible mechanism of varying graphene conductivity in contact with liquid may be also associated with the change in spatial orientation

of water molecules near the graphene surface, which was discussed in detail in [52]. In this study, a graphene sensor was fully immersed in water, which would have a much higher effect than from a single drop due to a different liquid contact area and graphene surface. This study explores a degree to which a graphene sensor is sensitive to water drops on its surface and whether a water drop evaporation behavior may be evaluated by the change in conductivity of the graphene sensor. Current studies are performed directly in the field of drying water drop behavior analysis, however, in future they may be supplemented by the analysis of behavior and composition of drying drops that contain a dispersion phase. Biological fluids may serve as an example of such systems. There are already studies that determine whether some typical markers [56] and diseases [57] exist by analyzing the structure of sediment of dry biological drops. The presence and composition of dispersion phase will obviously affect not only the sediment map structure, but also the liquid drop evaporation behavior. Consequently, one of the main potential graphene sensor application may involve creation of a relatively simple sensor on its basis that will be used to evaluate the composition of a biological fluid drop by evaporation behavior.

1. Samples and methods

Experimental study of drops was carried out in two stages. The first stage involved creation of graphene sensors that are sensitive to water drops on their surfaces. The second stage involved combined measurement of conductive properties of the sensors and configuration of water drops evaporating on their surface. Flow chart of the sequence of operations implemented during fabrication and utilization of graphene sensors is shown in Figure 1. Conductive properties of the sensors were measured using devices connected in series: the sensor to be fabricated, digital amperemeter (CA3010/3-232) and power supply (QJ12003E).

When sensors were fabricated, it was necessary to synthesize graphene on a copper substrate using the vapor-phase deposition method, transfer the graphene to a non-conducting substrate, SiO2 in our case, and to make conductive contacts. Let's discuss each of the intermediate operations in detail.

1.1. Graphene synthesis

Graphene synthesis on copper substrate was performed using an experimental system described in detail in [58]. Methane was used as carbon-containing gas. Before the synthesis stage, the 10×15 mm copper substrate was rinsed with acetone, ethanol and distilled water under ultrasound. After this, the sample was dried and placed into a gas chamber. The chamber was evacuated , then filled with argon and heated up to the annealing temperature (1070°C). Then the copper substrate was annealed during 30 min in hydrogen at a rate of 100 st.cm^3/min (standard cubic centimeter per minute). After the annealing stage, Ar (90 st.cm^3/min)+H_2 (20 st.cm^3/min)+CH_4 (0.2 st.cm^3/min) gas mixture was supplied to the chamber during 10 min at 1070°C.

1.2. Transferring graphene onto a substrate and fabricating contacts

Transfer of the graphene grown on the copper substrate carried out through liquid included the following three stages. First stage — substrate etching in $(NH_4)_2S_2O_8$ with a concentration of 0.044 g/mol during 24 h. The substrate was floating on the solution surface. Then after full copper dissolution, graphene film remained on the liquid surface. The second stage used a multiple bottom pumping method to substitute the $(NH_4)_2S_2O_8$ solution with distilled water. Multiple rinsing with distilled water leads to partial or full removal of functional groups associated with graphene. Samples were rinsed using a technique similar to that described in [59]. For this, four iterations were required. Third stage — catching the graphene films on the water surface and transferring the film onto the SiO_2 substrate. Graphene was transferred onto the substrates after rinsing and drying of the Si substrates in argon. This procedure is described in detail in [59].

After transferring the synthesized graphene onto the substrate, a mask with holes corresponding to the electrode sizes and positions was put on the sample. Then the copper electrodes were applied through the holes in the mask by the magnetron sputtering method. This was the end of the graphene sensor fabrication procedure. After the procedures, the sensor face consisted of 2−3- layer graphene applied to the Si substrate. For typical Raman spectra of the fabricated substrates, see [59].

1.3. Drop measurements

During evaporation of drops on the graphene sensors, geometrical properties of the drops were measured. i.e. height of drops, drop-to-sensor contact area, and stationary contact angles. Note that all experiments were carried out at approx. 25°C and relative humidity of approx. 50%. In these conditions, drop evaporation depending on their sizes took 1 h to 3 h. This circumstance made it possible to neglect the difference between the stationary contact angle and the outflowing contact angle [60]. Measurements were carried out using two HiView 50x−1600x digital microscopes that provided recording of the horizontal and front/lateral projections of the drops. Despite various types of surface roughness, that are discussed below, during evaporation on the horizontal surface, the drops preserved their axial symmetry most of the time, i.e. the front and lateral projections of the drops differed unessentially. The wetting angle was measured by the sessile drop method [61]. Further, angle values were measured by the tangential method [61]. All linear sizes of the drops that were needed to determine contact angles, heights, drop-to-surface contact

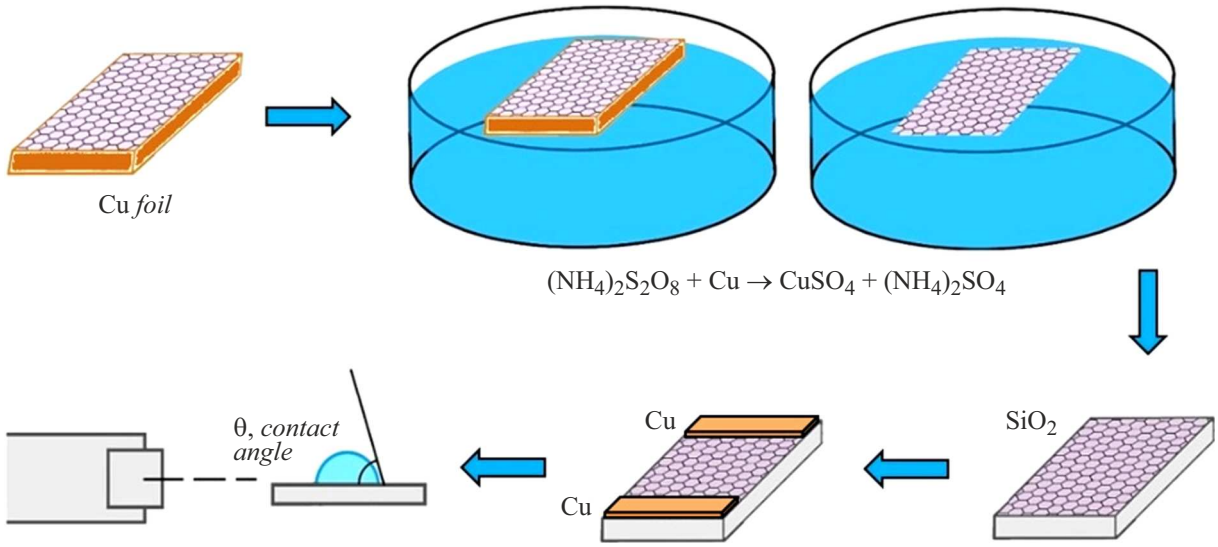

Figure 1. Flow chart of graphene sensor fabrication and utilization.

areas were found from processing the recorded images in ImageJ [62]. The main contribution to the geometry measurement error is made by the measurement of drop heights and contact angles. The absolute measurement error of drop height is approx. 0.025 mm and of contact angles is approx. 1°, which is attributable to the resolution of the used microscopes and image processing procedure in ImageJ. Consequently, the initial relative measurement error of these quantities is about 1%. Growth of relative errors proportional to the decrease in drop heights and contact angles is further observed. Distilled water per GOST 58144-2018 was used as the process liquid. Thus, the mass concentration in mg/dm^3 shall not exceed: for ammonium ions — 0.2, nitrate ions — 0.2, sulfate ions — 0.5, chloride ions — 0.5, total organic carbon — 0.5, Al — 0.05, Fe — 0.05, Ca — 0.8, Cu — 0.02, Pb — 0.05, Zn — 0.2. The presence of impurities led to irreversible increase in sensor resistance after complete drying of the drops. Therefore, these will be single-use sensors in real practical applications.

1.4. Conductive property measurement

Graphene chip resistance was measured by the flowing current and applied voltage. For the purpose of measurement, a constant voltage of 1.5 V was used, and the system current was measured. Resistance measurement error of the graphene chip was 1% max. System resistance uniformity was studied additionally, for which additional conductive tape electrodes were applied to the graphene, and then dependence of resistance on electrode spacing was measured. This procedure provided the linear dependence of resistance on electrode spacing. Deviation from the linear dependence was max. 5%, which was mainly attributable to the electrode positioning accuracy. Thus, the graphene chip resistance may be considered as uniform.

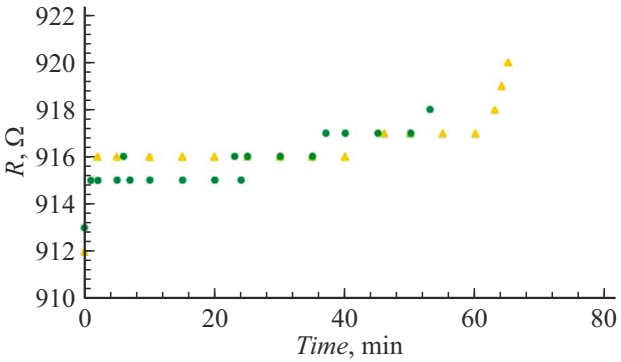

Figure 2. Dependences of resistance on time for 5 μl water drops applied to various points on the graphene sensor. Triangles corresponded to the center of drop placed at 1.5 mm from the electrode, circles corresponded to the center of drop placed at 5 mm from the electrode.

2. Findings and discussion

This study used sensors that had a certain difference in initial resistance$R$. The initial resistance of sensors was approx. $1000 \pm 200\,\Omega$. Graphene surface area was approx. 1 cm^2. When 5 μl water drops were applied, sensor resistance changed by approx. $6-8\,\Omega$ (Figure 2), which may be considered as not very substantial compared with the total resistance of a dry sensor. In Figure 2 and in all discussions hereinafter, the sensor resistance will mean total resistance of the drop −graphene sensor system.

However, sensor sensitivity to drops was determined even on such relatively small drops. Dependence of resistance variation on drop positions on the sensors (closer or farther to/from an electrode) was also verified. Significant dependence on water drop position wasn't detected (Figure 2). Main experiments were conducted on 50 μl water drops.

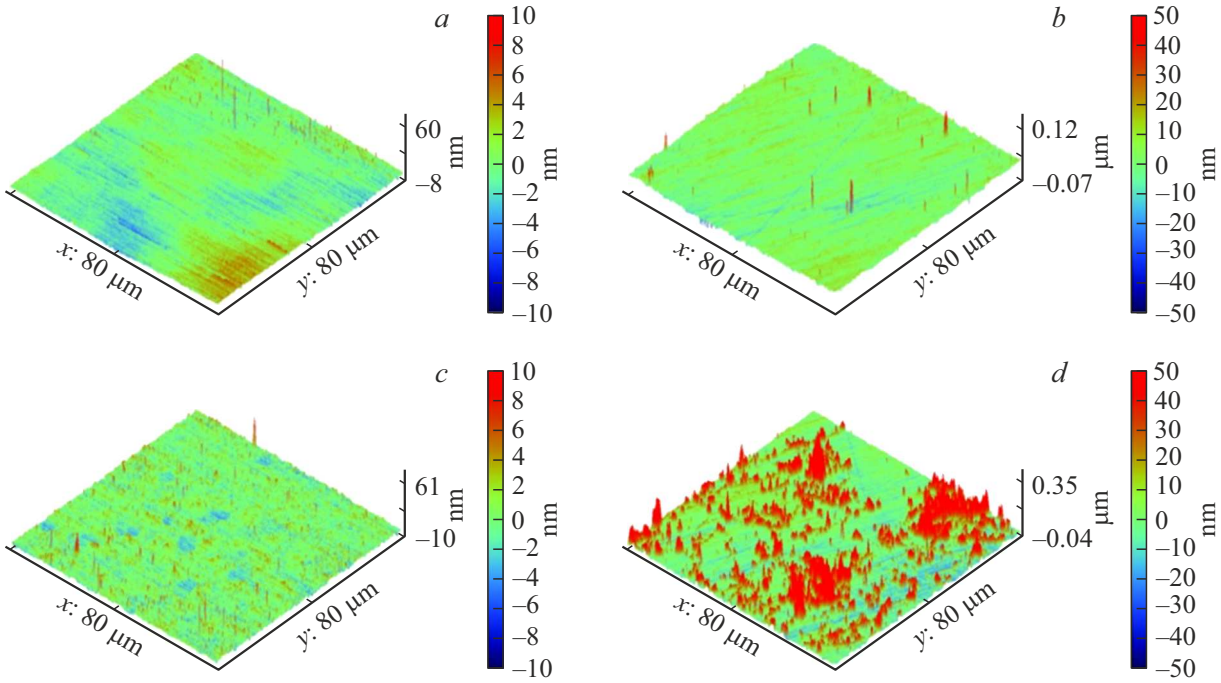

Figure 3. Images of SiO_2 substrates with different surface roughness recorded using a scanning probe microscope; *a, b* — correspond to substrate surfaces before graphene deposition, *c, d* — correspond to substrate surfaces after graphene deposition.

When drops with this volume were applied to the surface, they occupied approximately 1/3 of the working surface of the sensors. When a drop was applied to a sensor, the drop−sensor system resistance reduced by 50−60 Ω during 60−180 s. Then, when the drop evaporated, the total resistance of the drop−sensor system only increased. For all time dependences shown below, observation started 100 s after drop application. For the drops studied here, sensor resistance variation from the start of observation to complete drying was approx. 200−300 Ω.

This work addressed non-conductive oxidized silicon substrate with different roughness degrees. Substrates with different roughness were used in order to obtain substantially different drop evaporation conditions. They may include conditions with resting, smoothly moving and breaking contact line of the drop. Typical illustrations of the corresponding surfaces obtained using a scanning probe microscope are shown in Figure 3.

For a smoother surface, rms deviation of the profile from the middle line is Rms = 1.6 nm (Figure 3, *a*), for a rougher surface, Rms = 5.8 nm (Figure 3, *b*). After graphene application, surface characteristics varied to Rms = 2.8 nm (Figure 3, *c*) and Rms = 23.1 nm (Figure 3, *d*), respectively. Similarly, for a smoother surface and for a rougher surface, mean deviation of profile from the middle line is Ra = 1.1 nm and Ra = 4.3 nm, respectively. After graphene application, surface characteristics varied to Ra = 1.5 nm and Ra = 13.6 nm, respectively. For resistance measurement of evaporating water drops, significantly different dependences of sensor resistances on time were found on such sensors (Figure 4).

In both cases increase in resistance was observed. For a less rough sample, two typical sections $R(t)$ that are close to linear sections may be distinguished. Further, three typical sections may be distinguished on $R(t)$for a rougher sample.

Figure 5, 6 shows illustrations of evaporating drops at various typical times.

To find the correlation between the sensor resistance variation and water drop evaporation behavior, we first consider the geometrical property variation of drops with time and their interconnection with each other.

As in the case with the dependences of sensor resistance on time (Figure 4), some typical sections can be also highlighted on the dependences of drop heights on time

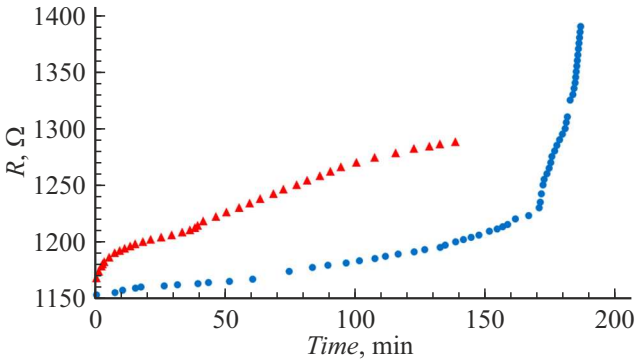

Figure 4. Dependences of resistances on time or drops applied to graphene sensors. Red triangles correspond to a surface with Rms = 23.1 nm, blue circles correspond to a surface with Rms = 2.8 nm.

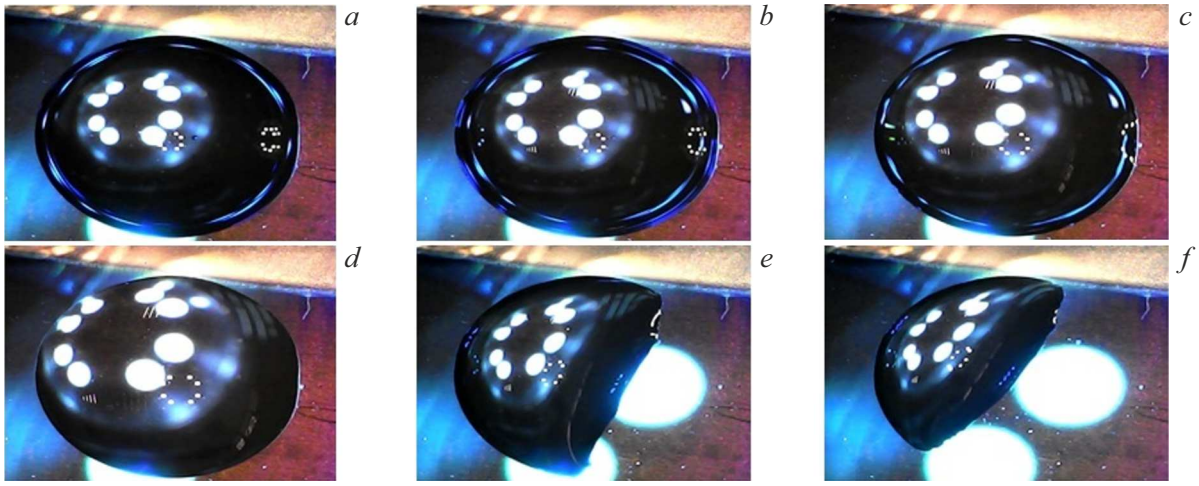

Figure 5. Drop evaporation on a surface characterized by Rms = 2.8 nm. Cases $a-f$ correspond to 0, 50, 100, 150, 170, 180 min after the start of observation of drop evaporation; with cases e, f corresponding to the drop contact line breaking condition.

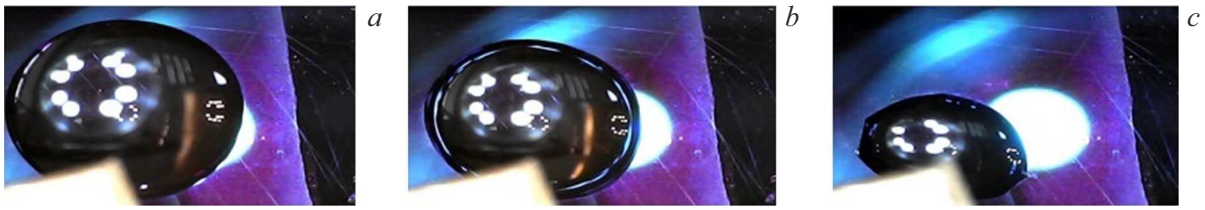

Figure 6. Drop evaporation on a surface characterized by captionRms = 23.1 nm. Cases $a-c$ correspond to 0, 50, 100 min after the start of observation of drop evaporation.

(Figure 7, a), contact angles of drops on time (Figure 7, b) and drop-to-surface contact areas on time (Figure 7, c).

Thus, for a smoother sample, two sections with linear decrease in height proportionally to the contact angle were observed, the corresponding data is shown in Figure 7, d.

These curves differ only in their inclination, which is corresponded by a faster decrease in height at the final drop drying stage. For a rougher sample, three typical evolution stages were observed. Two of them had linear decrease in height proportional to the contact angle. Decrease in height without change in the contact angle was observed on an intermediate section. To understand the sections to which drop evaporation behavior stages correspond, we also consider the dependences of contact areas of drops with the graphene surface (Figure 7, c).

Two typical sections correspond to drop evaporation on a smoother sample. The first section — with insignificant drop-to-sensor contact area variation, the second section — with sharp decrease in the contact area. Thus, two dynamic modes were observed on a smoother sample. The first mode corresponds to drop evaporation with proportional decrease in drop height and contact angle, but with unchanged drop-to-surface contact area and contact line position. In the second mode, when a certain critical contact angle was achieved, the contact line was broken sharply, and the remaining small drop evaporated quickly as the height, contact angle and drop-to-surface contact area decreased. In Figure 4, sharp growth of sensor resistance corresponds to switching between these two evaporation modes. Let's perform the same analysis for the rougher sample. Dependence of the drop-to-surface contact area on time for the sample has two typical sections, a small initial section with insignificant contact area variation, and a section with linear decrease in the contact areas with time (Figure 7, c). Taking into account the height, contact angle and drop-to-surface contact area covariations, three typical evaporation stages may be distinguished for a drop on the rougher surface. The first stage is equivalent to that on the smoother sample, i.e. the drop height and contact angle decrease, while the drop-to surface contact areas remains unchanged. The main difference from the smoother sample here was in much shorter duration of this stage. Then, contact line started moving and the drop-to-surface contact area decreased accordingly. However, unlike the smoother sample, the contact line moved smoothly without significant breaks. At this evaporation stage, the drop height continued decreasing with almost constant contact angle. The last evaporation stage was accompanied by simultaneous decrease in the drop height, contact angle and drop-to-surface contact area. At this stage, smooth movement of the contact line usually changed to its break. As for the drop evaporating on the smoother surface, all

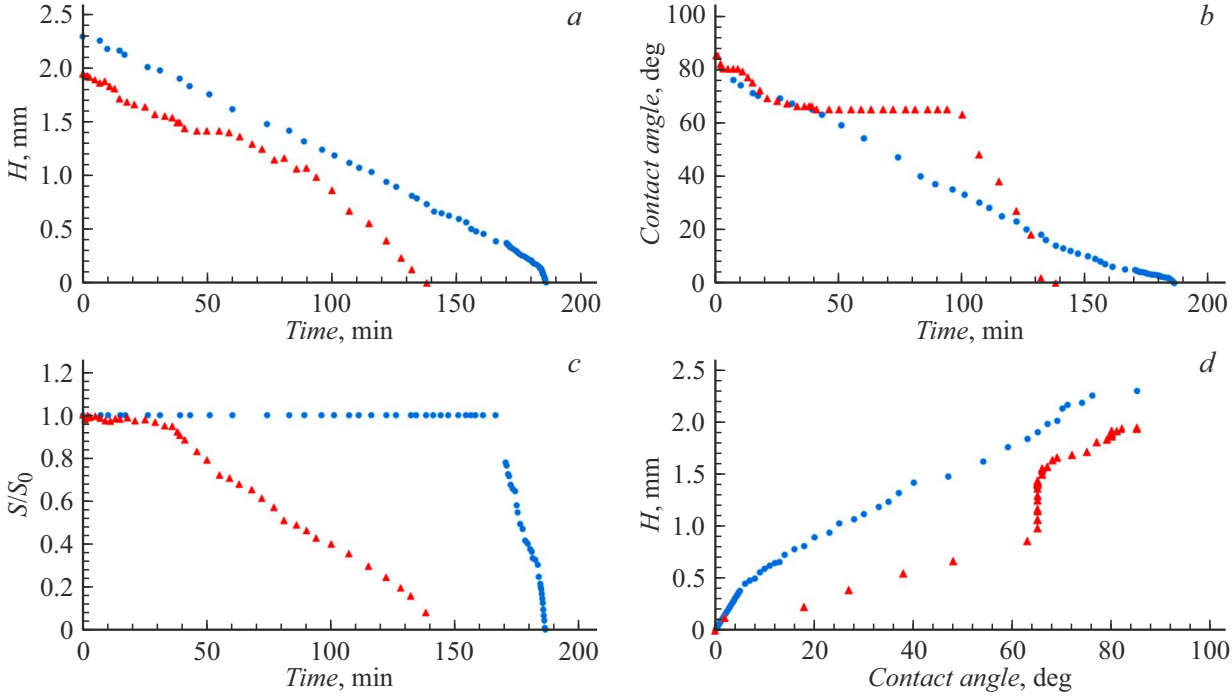

Figure 7. Dependences on time: *a* — of drop heights, *b* — contact angles of drops, *c* — drop-to-surface contact areas (contact areas are normalized to contact areas at the start of observation of drop evaporation), *d* — dependences of drop heights on their contact angles. In all cases, red triangles correspond to a surface with Rms = 23.1 nm, blue circles correspond to a surface with Rms = 2.8 nm.

three evaporation stages were accompanied by variation of $R(t)$ (Figure 4). Note also that the contact line was broken on the sensor with smoother surface much earlier than on rougher surfaces. This is presumably attributable to a better adhesion of the water drop to the less rough surface. At the final drop evaporation stages accompanied by the contact line break, loss of axial symmetry of the evaporating drops was also observed , which corresponds to the cases shown in Figure 5, *e,f.*

As a result, variation of drop evaporation conditions on different substrates may be determined using graphene sensors. Let's consider separately the dependences of evaporating drop geometry on sensor resistances (Figure 8).

The sensor turns out to be sensitive to each of these quantities and quantity variation. These quantities are certainly interconnected and their variation may be correlated. However, the drop evaporation behavior variation expressed in the variation of the rate of change of one of the studied geometrical parameters is reflected in $R(t)$. Simultaneous analysis of the time dependences of drop geometry and sensor resistances for various practical cases can be potentially used to recover curves equivalent to curves shown in Figure 8.

This study also verified reproducibility of results. The results shown above demonstrate irreversible resistance growth as the drop gets dry, which is presumably associated with the presence of impurities in the distilled water. Moreover, the irreversible change in sensor resistance may be associated with atmospheric hydrocarbons deposited on the sensor and drop surface during the experiment. When the sensor was re-used in conditions that were similar in temperature and moisture, the obtained dependences of sensor resistance on time were reproduced with an accuracy of 10–15% taking into account the correction for initial sensor resistance. When using different sensors with close roughnesses, qualitative agreement between the results was observed. Quantitative difference occurred in the initial sensor resistances. During correction of curves for initial resistances (initial resistances are assumed to be equal), the difference between resistance variations was 10–20%.

Conclusion

The study investigated whether the graphene sensor was applicable to determine geometrical properties of water drops evaporating on it. SiO_2 substrates with different roughnesses were examined. Different drop drying behaviors were observed on these substrates coated with graphene applied by the vapor-phase deposition method. It was found that the drop evaporation conditions characterized by particular ratios of drop height, contact angle and drop-to-surface contact area variations can be determined by the dependences of sensor resistances on time. These dependences may be useful for creating devices that use sensor properties of graphene. These devices may potentially include sensors that detect drops on the surface

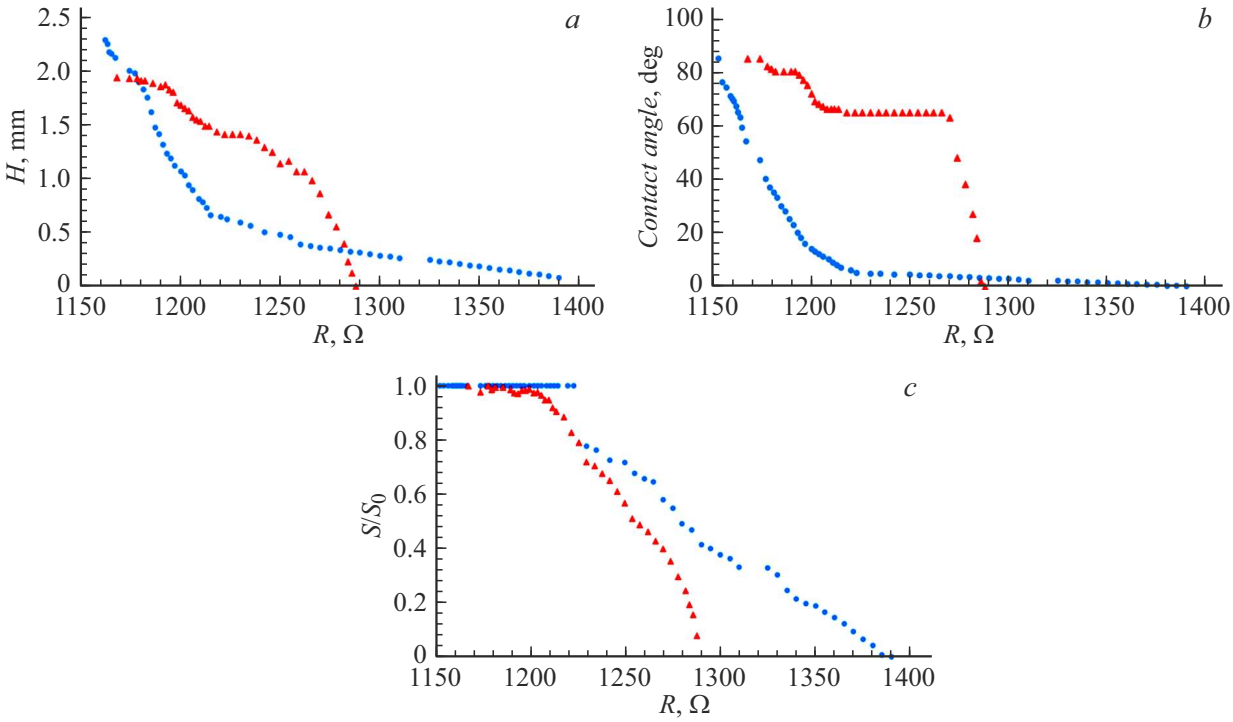

Figure 8. Dependences on drop−sensor resistances:of drop heights *a* , contact angles of drops *b*, drop-to-surface contact areas *c* (contact areas are normalized to contact areas at the start of observation of drop evaporation). In all cases, red triangles correspond to a surface with Rms = 23.1 nm, blue circles correspond to a surface with captionRms = 2.8 nm.

of various installations or dry spots during liquid film boiling on the heater surfaces. Such sensors can be also used to evaluate the parameters of evaporating drops in areas inaccessible for optical measurement. Biomedical applications are one of the most promising areas of potential utilization of such sensors. Evaporation behavior of biological fluids is known to depend significantly on their composition. It is shown that the graphene sensor can track this behavior for relatively small water drops. Moreover, the graphene sensor may have a higher sensitivity to separate components of drops of biological origin. Sensitivity of such sensors to separate components of biological drops may be increased by preliminary functionalization of graphene with various elements and structures.

Conflict of interest

The authors declare no conflict of interest.

References

[1] M. Javaid, A. Haleem, Sh. Rab, R.P. Singh, R. Suman. Sen. Int., **2**, 100121 (2021). DOI: 10.1016/j.sintl.2021.100121
[2] Sh. Dhall, B.R. Mehta, A.K. Tyagi, K. Sood. Sen. Int., **2**, 100116 (2021). DOI: 10.1016/j.sintl.2021.100116
[3] F. Costa, S. Genovesi, M. Borgese, A. Michel, F.A. Dicandia, G. Manara. Sensors, **21** (9), 3138 (2021). DOI: 10.3390/s21093138
[4] N. Wen, L. Zhang, D. Jiang, Z. Wu, B. Li, C. Suna, Z. Guo. J. Mat. Chem. A, **8** (48), 25499 (2020(2021)). DOI: 10.1039/D0TA09556G
[5] A. Nag, A. Mitra, S.C. Mukhopadhyay. Sens. Actuators A Phys., **270**, 177 (2018). DOI: 10.1016/j.sna.2017.12.028
[6] J. Liu, S. Bao, X. Wang. Micromachines, **13** (2), 184 (2022). DOI: 10.3390/mi13020184
[7] G. Li, G. Hong, D. Dong, W. Song, X. Zhang. Adv. Mater., **30**, 1801754 (2018). DOI: 10.1002/adma.201801754
[8] Z. Yang, L. Wang, W. Sun, S. Li, T. Zhu, W. Liu, G. Liu. Appl. Surf. Sci., **401**, 146 (2017). DOI: 10.1016/j.apsusc.2017.01.009
[9] S.S.A. Kumar, S. Bashir, S.K. Ramesh, S.A. Ramesh. Flat. Chem., **31**, 100326 (2022). DOI: 100326.10.1016/j.flatc.2021.100326
[10] A.K. Geim, K.S. Novoselov. Nat. Mater., **6** (3), 183 (2007). DOI: 10.1038/nmat1849
[11] E.W. Hill, A. Vijayaragahvan, K. Novoselov. IEEE Sens. J., **11** (12), 3161 (2011). DOI: 10.1109/JSEN.2011.2167608
[12] Q. He, Sh. Wu, Z. Yina, H. Zhang. Chem. Sci., **3** (6), 1764 (2012). DOI: 10.1039/C2SC20205K
[13] Y. Liu, X. Dong, P. Chen. Chem. Soc. Rev., **41** (6), 2283 (2012). DOI: 10.1039/C1CS15270J
[14] T. Kuila, S. Bose, P. Khanra, A.K. Mishra, N.H. Kim, J.H. Lee. Biosens. Bioelectron., **26** (12), 4637 (2011). DOI: 10.1016/j.bios.2011.05.039
[15] Yu. Zhang, Y.-W. Tan, H.L. Stormer, Ph. Kim. Nature, **438** (7065), 201 (2005). DOI: 10.1038/nature04235
[16] K.S. Novoselov, A.K. Geim, S.V. Morozov, D. Jiang, M.I. Katsnelson, I.V. Grigorieva, S.V. Dubonos, A.A. Firsov. Nature, **438** (7065), 197 (2005). DOI: 10.1038/nature04233

[17] M. Pumera, A. Ambrosi, A. Bonanni, E.L.Kh. Chng, H.L. Poh. Trends Analyt. Chem., **29** (9), 954 (2010). DOI: 10.1016/j.trac.2010.05.011
[18] F. Schedin, A.K. Geim, S.V. Morozov, E.W. Hill, P. Blake, M.I. Katsnelson, K.S. Novoselov. Nat. Mater., **6** (9), 652 (2007). DOI: 10.1038/nmat1967
[19] X. Xu, Ch. Liu, Zh. Sun, T. Cao, Zh. Zhang, E. Wang, Zh. Liu, K. Liu. Chem. Soc. Rev., **47** (9), 3059 (2018). DOI: 10.1039/C7CS00836H
[20] E. Voloshina, D. Usvyat, M. Schütz, Yu. Dedkov, B. Paulus. Phys. Chem. Chem. Phys., **13** (25), 12041 (2011). DOI: 10.1039/C1CP20609E
[21] D.W. Boukhvalov, M.I. Katsnelson. J. Phys. Condens. Matter, **21** (34), 344205 (2009). DOI: 10.1088/0953-8984/21/34/344205
[22] C. Zhang, L. Fu, N. Liu, M. Liu, Y. Wang, Z. Liu. Adv. Mater., **23** (8), 1020 (2011). DOI: 10.1002/adma.201004110
[23] U.N. Maiti, W.J. Lee, J.M. Lee, Y. Oh, J.Y. Kim, J.E. Kim, J. Shim, T.H. Han, S.O. Kim. Adv. Mater., **26** (1), 40 (2014). DOI: 10.1002/adma.201303265
[24] V. Georgakilas, M. Otyepka, A.B. Bourlinos, V. Chandra, N. Kim, K.Ch. Kemp, P. Hobza, R. Zboril, K.S. Kim. Chem. Rev., **112** (11), 6156 (2012). DOI: 10.1021/cr3000412
[25] A.D. Smith, K. Elgammal, F. Niklaus, A. Delin, A.C. Fischer, S. Vaziri, F. Forsberg, M. Råsander, H. Hugosson, L. Bergqvist, S. Schröder, S. Kataria, M. Östlinga, M.C. Lemme. Nanoscale, **7**, 19099 (2015). DOI: 10.1039/C5NR06038A
[26] O. Leenaerts, B. Partoens, F.M. Peeters. Microelectronics J., **40** (4-5), 860 (2009). DOI: 10.1016/j.mejo.2008.11.022
[27] F. Yavari, Ch. Kritzinger, Ch. Gaire, Li Song, H. Gulapalli, Th. Borca-Tasciuc, P.M. Ajayan, N. Koratkar. Small, **6** (22), 2535 (2010). DOI: 10.1002/smll.201001384
[28] T.O. Wehling, A.I. Lichtenstein, M.I. Katsnelson. Appl. Phys. Lett., **93** (20), 202110 (2008). DOI: 10.1063/1.3033202
[29] C.E. Giusca, V. Panchal, M. Munz, V.D. Wheeler, L.O. Nyakiti, R.L. Myers-Ward, D.K. Gaskill, O. Kazakova. Adv. Mater. Interf., **2** (16), 1500252 (2015). DOI: 10.1002/admi.201500252
[30] Yu. Liu, H. Liu, Y. Chu, Y. Cui, T. Hayasaka, V. Dasaka, L. Nguyen, L. Lin. Adv. Mater. Interf., **5** (9), 1701640 (2018). DOI: 10.1002/admi.201701640
[31] R.M. Ribeiro, N.M.R. Peres, J. Coutinho, P.R. Briddon. Phys. Rev. B, **78** (7), 075442 (2008). DOI: 10.1103/PhysRevB.78.075442
[32] O. Leenaerts, B. Partoens, F.M. Peeters. Phys. Rev. B., **77** (12), 125416 (2008). DOI: 10.1103/PhysRevB.77.125416
[33] O. Leenaerts, B. Partoens, F.M. Peeters. Phys. Rev. B, **79** (23), 235440 (2009). DOI: 10.1103/PhysRevB.79.235440
[34] X. Li, Ji Feng, E. Wang, Sh. Meng, J. Klimeš, A. Michaelides. Phys. Rev. B, **85** (8), 085425 (2012). DOI: 10.1103/PhysRevB.85.085425
[35] C. Melios, C.E. Giusca, V. Panchal, O. Kazakova. 2D Materials, **5** (2), 022001 (2018). DOI: 10.1088/2053-1583/aa9ea9
[36] M.H. Bagheri, R.T. Loibl, J.A. Boscoboinik, S.N. Schiffres. Carbon, **155**, 580 (2019). DOI: 10.1016/j.carbon.2019.08.083
[37] M.F. Craciun, S. Russo, M. Yamamoto, S. Tarucha. NanoToday, **6** (1), 42 (2011). DOI: 10.1016/j.nantod.2010.12.001
[38] J. Ma, A. Michaelides, D. Alfè, L. Schimka, G. Kresse, E. Wang. Phys. Rev. B, **84** (3), 033402 (2011). DOI: 10.1103/PhysRevB.84.033402
[39] H. Wang, G. Yu. Adv. Mater., **28** (25), 4956 (2016). DOI: 10.1002/adma.201505123
[40] Ch. Melios, A. Centeno, A. Zurutuza, V. Panchal, C.E. Giusca, S. Spencer, S.R.P. Silva, O. Kazakova. Carbon, **103**, 273 (2016). DOI: 10.1016/j.carbon.2016.03.018
[41] W.L. Tong, Ye.M. Hung, H. Yu, M.K. Tan, B.Th. Ng, B.Th. Tan, H.A. Wu, A.K. Soh. Adv. Mater. Interf., **5** (13), 1800286 (2018). DOI: 10.1002/admi.201800286
[42] Y. Han, Z. Xu, C. Gao. Adv. Func. Mater., **23** (29), 3693 (2013). DOI: 10.1002/adfm.201202601
[43] M.-F. Li, Y.-G. Liu, G.-M. Zeng, N. Liu, Sh.-Bo Liu. Chemosphere., **226**, 360 (2019). DOI: 10.1016/j.chemosphere.2019.03.117
[44] J. Feng, Z. Guo. Nanoscale horiz., **4** (2), 339 (2019). DOI: 10.1039/C8NH00348C
[45] C.J. Shih, M.S. Strano, D. Blankschtein. Nat. Mater., **12** (10), 866 (2013). DOI: 10.1038/nmat3760
[46] F. Taherian, V. Marcon, N.F.A. van der Vegt, F. Leroy. Langmuir, **29** (5), 1457 (2013). DOI: 10.1021/la304645w
[47] K. Xia, M. Jian, W. Zhang, Yi. Zhang. Adv. Mater. Interf., **3** (6), 1500674 (2016). DOI: 10.1002/admi.201500674
[48] A. Kayal, A. Chandra. J. Phys. Chem. C, **123** (10), 6130 (2019). DOI: 10.1021/acs.jpcc.9b01040
[49] Q. Li, Yi. Xiao, Xi. Shi, Sh. Song. Nanomaterials, **7** (9), 265 (2017). DOI: 10.3390/nano7090265
[50] Yi. Zhang, H.B. de Aguiar, J.T. Hynes, D. Laage. J. Phys. Chem. Lett., **11** (3), 624 (2020). DOI: 10.1021/acs.jpclett.9b02924
[51] L.B. Dreier, Z. Liu, A. Narita, M.-J. van Zadel, K. Müllen, K.-J. Tielrooij, E.H.G. Backus, M. Bonn. J. Phys. Chem. C, **123** (39), 24031 (2019). DOI: 10.1021/acs.jpcc.9b05844
[52] V. Andryushchenko, D. Sorokin, M. Morozova, O. Solnyshkina, D. Smovzh. Appl. Surf. Sci., **567**, 150843 (2021). DOI: 10.1016/j.apsusc.2021.150843
[53] D.V. Sorokin, D.A. Shatilov, V.A. Andryushchenko, M.S. Makarov, V.S. Naumkin, D.V. Smovzh. Thermophys. Aerom., **29** (6), 899 (2022). DOI: 10.1134/S0869864322060099
[54] W. Xu, Yu. Song, R.X. Xu, Z. Wang. Adv. Mater. Interf., **8** (2), 2000670 (2021). DOI: 10.1002/admi.202000670
[55] M. Lizée, A. Marcotte, B. Coquinot, N. Kavokine, K. Sobnath, C. Barraud, A. Bhardwaj, B. Radha, A. Niguès, L. Bocquet, A. Siria. Phys. Rev. X, **13** (1), 011020 (2022). DOI: 10.1103/PhysRevX.13.011020
[56] J.T. Wen, C.M. Ho, P.B. Lillehoj. Langmuir, **29** (26), 8440 (2013). DOI: 10.1021/la400224a
[57] J.M. Cameron, H.J. Butler, D.S. Palmer, M.J. Baker. J. Biophotonics, **11** (4), e201700299 (2018). DOI: 10.1002/jbio.201700299
[58] I.A. Kostogrud, E.V. Boyko, D.V. Smovzh. Mater. Chem. Phys., **219**, 67 (2018). DOI: 10.1016/j.matchemphys.2018.08.001
[59] V.A. Andryushchenko, D.V. Sorokin, I.A. Betke, S.V. Komlina, S.V. Starinskiy, M.M. Vasiliev, E.A. Maximovskiy, M.N. Khomyakov, D.V. Smovzh. J. Mol. Liqu., **395**, 123827 (2024). DOI: 10.1016/j.molliq.2023.123827

[60] S. Herminghaus, M. Brinkmann, R. Seemann. Annu. Rev. Mater. Res., **38** (1), 101 (2008). DOI: 10.1146/annurev.matsci.38.060407.130335
[61] D.N. Staicopolus. J. Colloid Sci., **17** (5), 439 (1962). DOI: 10.1016/0095-8522(62)90055-7
[62] C.A. Schneider, W.S. Rasband, K.W. Eliceiri. Nat. Meth., **9** (7), 671 (2012). DOI: 10.1038/nmeth.2089

Translated by E.Ilinskaya